Journal Pre-proof

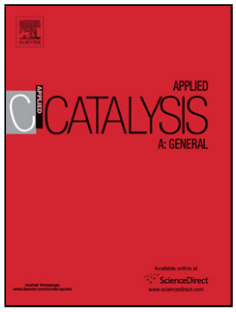

Successive vapour phase Guerbet condensation of ethanol and 1-butanol over Mg-Al oxide catalysts in a flow reactor

Olga V. Larina, Karina V. Valihura, Pavlo I. Kyriienko, Nina V. Vlasenko, Dmytro Yu. Balakin, Ivan Khalakhan, Tomaž Čendak, Sergiy O. Soloviev, Svitlana M. Orlyk

PII: S0926-860X(19)30420-X

DOI: https://doi.org/10.1016/j.apcata.2019.117265

Reference: APCATA 117265

To appear in: *Applied Catalysis A, General*

Received Date: 27 June 2019

Revised Date: 6 September 2019

Accepted Date: 19 September 2019

Please cite this article as: Larina OV, Valihura KV, Kyriienko PI, Vlasenko NV, Balakin DY, Khalakhan I, Čendak T, Soloviev SO, Orlyk SM, Successive vapour phase Guerbet condensation of ethanol and 1-butanol over Mg-Al oxide catalysts in a flow reactor, *Applied Catalysis A, General* (2019), doi: https://doi.org/10.1016/j.apcata.2019.117265

Successive vapour phase Guerbet condensation of ethanol and 1-butanol over Mg-Al oxide catalysts in a flow reactor

Olga V. Larina[a*], Karina V. Valihura[a], Pavlo I. Kyriienko[a*], Nina V. Vlasenko[a], Dmytro Yu. Balakin[b], Ivan Khalakhan[c], Tomaž Čendak[d], Sergiy O. Soloviev[a] and Svitlana M. Orlyk[a]

[a]L.V. Pisarzhevsky Institute of Physical Chemistry of the NAS of Ukraine, 31 Prosp. Nauky, 03028 Kyiv, Ukraine.

[b]Institute of Physics of the NAS of Ukraine, 46 Prosp. Nauky, 03028 Kyiv, Ukraine.

[c]Charles University, Faculty of Mathematics and Physics, Department of Surface and Plasma Science, V Holešovičkách 2, 18000 Prague, Czech Republic.

[d]National Institute of Chemistry, Department of Inorganic Chemistry and Technology, Hajdrihova 19, 1001 Ljubljana, Slovenia.

*Corresponding authors, e-mail: olga.larina@ukr.net; pavlo_kyriienko@ukr.net

Graphical abstract

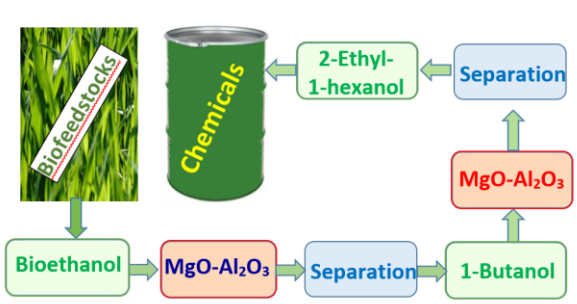

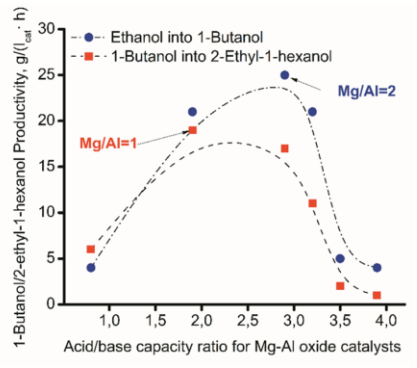

Highlights

- Vapour phase condensation of 1-butanol to 2-ethyl-1-hexanol over Mg-Al oxide solid catalysts in flow under atmospheric pressure have been performed for the first time.
- Experimental opportunities for production of 2-ethyl-1-hexanol from ethanol in a flow reactor under atmospheric pressure by successive Guerbet condensation over Mg-Al oxide catalysts has been shown.
- The selectivity and yield of the main products in the process strong depends of acid/base capacity ratio, which is determined by a Mg/Al ratio.
- Optimal Mg/Al ratio and arrangement of surface active sites are different for the reacting alcohols with different carbon chain length.

ABSTRACT:

The successive vapour phase condensation of ethanol and 1-butanol (via Guerbet reaction) in a flow reactor under atmospheric pressure was studied over catalytic Mg-Al oxide compositions. Wherein the vapour phase condensation of 1-butanol to 2-ethyl-1-hexanol in flow has been investigated for the first time. The acid/base capacity ratio, which is determined by the Mg/Al ratio, is an important characteristic for the activity and selectivity of Mg-Al oxide catalysts in the abovementioned processes. The carbon chain length of the reacting alcohols, an arrangement of surface active sites and other steric factors also have an impact on Guerbet

condensation in the vapour phase. High productivity of Mg-Al oxide system to the Guerbet alcohols: 1-butanol – 25 g/(L_{cat}·h), 2-ethyl-1-hexanol – 19 g/(L_{cat}·h), has been achieved. The results have shown a prospect of successive conversion realization: 1) ethanol → 1-butanol; 2) 1-butanol → 2-ethyl-1-hexanol for the production of 2-ethyl-1-hexanol from ethanol.

KEYWORDS: Guerbet condensation, ethanol, 1-butanol, 2-ethyl-1-hexanol, flow reactor, vapour phase, Mg-Al oxide system

1. Introduction

Development of technologies for bio-ethanol upgrade into valuable chemicals and fuels is an important issue in sustainable chemistry studies [1–3]. Ethanol is a flexible building block for biorefinaries and can be used for the direct production of ethylene, propylene, 1,3-butadiene and hydrocarbons, as well as for the production of oxygenated molecules, such as ethyl acetate, acetic acid, 1-butanol, etc. Moreover, ethanol production has been steadily increasing over the last decades [4].

2-Ethyl-1-hexanol (2-EH) is the most widely applied compound among C_6–C_{11} group of higher alcohols. It is generally used in the production of plasticisers (dioctyl terephthalate, phthalate, adipate), soaps, solvents, diesel additives and other special chemicals [5]. The well-known industrial process of 2-EH production based on Guerbet coupling reaction (Scheme 1) [6–8] involves exploitation of a batch reactor with homogeneous-heterogeneous catalytic systems (liquid base + solid noble metal) [9–12]. This technology is associated with number of drawbacks: expensive separation,

purification, recovery and waste treatment sections and a requirement for noble metal catalysts. Furthermore, water produced during Guerbet reaction leads to deactivation of the liquid alkali catalyst, incomplete conversion of alcohols and formation of by-products [13].

Scheme 1, near here

Catalytic conversion of bio-ethanol (EtOH) into higher alcohols via C-C coupling has attracted a scientific interest in recent years [1–4,14,15]. Dias et al. [16] have developed a techno-economic analysis of prospect for 1-butanol (BuOH) production from bio-ethanol by means of Guerbet condensation in a vapour phase plug flow reactor. The authors have identified the main parameters (lower reactor investment costs, less rigorous requirements for safety and shorter total operation period) allowing this process to be more effective in comparison to the liquid phase synthesis. The conversion of EtOH to BuOH in a flow over mixed oxide system is an already known process [17]. Patel et al. [18] have analysed techno-economic aspects of the catalytic production of 2-EH from ethanol in a flow system in the presence of solid catalysts. According to their research the process of producing 2-EH by means of staged condensation (1) EtOH → BuOH, 2) BuOH → 2-EH) may be a cost-effective alternative to the traditional industrial method.

A self-condensation of n-butanal to 2-EH has been widely investigated. Hamilton et al. [19] have reported the n-butanal aldol condensation and further selective hydrogenation of 2-ethyl-2-hexanal to 2-EH in the presence of $Pd/Na/SiO_2$ catalyst in a fixed bed reactor with high selectivity of 2-EH (94.9% at the conversion of 42.4%). Li et al. [20] have investigated the effect of reaction conditions on the one-pot sequential synthesis of 2-EH catalysed by $Ni/La{-}Al_2O_3$ in a self-condensation reaction conducted at 453 K for 8 h, and a further hydrogenation reaction conducted at 453 K for 6 h under 4

MPa; n-butanal conversion attains 100 % with 2-EH selectivity of 67%. Liang et al. [21] have reported the condensation of n-butanal to 2-EH over Ni/Ce−Al_2O_3 catalysts at 443 K, under 4 MPa and a reaction time of 8 h with full 100 % conversion of n-butanal and 66.9 % selectivity of 2-EH. However, an evaluation on reusability of Ni/Ce−Al_2O showed that the recovered sample lost its catalytic activity for hydrogenation due to deactivation of Ni species by the flaky boehmite γ-AlO(OH) formed from the hydration of γ-Al_2O_3. Patankar and Yadav [22] have performed the cascade engineered synthesis of 2-EH in a one pot from n-butanal under solventless conditions with a trifunctional mixed metal oxide catalyst containing 5 % Cu and MgO-Al_2O_3 (Mg/Al = 3) with 90 % selectivity. The reaction rate constants have been calculated for this process and aldol condensation are found to be a rate-controlling step.

There are few publications in the literature about one-pot direct synthesis of 2-EH from BuOH in an autoclave in the presence of expensive palladium or iridium complexes in combination with sodium butoxide as co-catalysts [23–26]. A vapour-phase condensation flow system and the use of non-precious metals catalysts are more responsive to current trends of sustainability processes. For realization of BuOH conversion to 2-EH in a flow reactor in a gaseous phase, heterogeneous acid-base catalysts are required.

Mg-Al mixed oxide catalysts derived from hydrotalcite (layered double hydroxides) precursors have received a great attention [27–31] as a very promising catalysts for the Guerbet condensation due to tuneable bifunctional acid–base properties, high surface area, high quantity of defects, structural stability both at high temperatures and in aqueous solutions, absence of toxic metals and relatively cheap cost. A number of works [32,33] have reported the importance of Mg/Al ratio in the catalyst.

In the present work, a principal possibility of producing 2-EH from EtOH by successive conversion: 1) EtOH → BuOH, 2) BuOH → 2-EH, in a flow reactor under atmospheric pressure in the presence of Mg-Al oxide catalysts is presented. The effects of Mg/Al ratio as well as temperature and liquid hourly space velocity on the catalytic properties of Mg-Al oxide systems are discussed.

2. Material and methods

2.1 Catalysts preparation

Mg-Al hydrotalcites with Mg/Al molar ratio of 1, 2, 3 and 4 were synthesized by the co-precipitation method under conditions of high super saturation (pH 10–12). 1M solutions of $Mg(NO_3)_2 \cdot 6H_2O$ and $Al(NO_3)_3 \cdot 9H_2O$ in various proportions were dropped into 200 mL of a buffer solution containing 1.6 M NaOH and 0.1 M Na_2CO_3 under vigorous stirring at temperature of 358 K. The mixture was kept at 358 K for 24 hours prior to a filtration step. The same method was used for MgO and Al_2O_3 synthesis. Then, the precipitates were separated by hot filtration, washed several times with warm deionized water to remove alkali metals and nitrate ions until neutral pH was reached, and dried at 393 K for 6 h. The resulting hydrotalcites were calcined at 873 K for 5 hours to obtain mixed oxides. This treatment temperature of Mg-Al hydrotalcites was chosen as optimal according to the work [27].

2.2. Catalysts characterization

XRD patterns of the powder samples were recorded using D8 Advance (Bruker AXS GmbH, Germany) diffractometer with monochromatized Cu-Kα radiation (nickel filter, $\lambda = 0.154$ nm).

Morphology of the samples was observed by means of Scanning Electron Microscopy (SEM) using a Tescan MIRA 3 microscope operating at 30 keV electron beam energy. Chemical composition mapping analysis was carried out using energy dispersive X-ray spectroscopy (EDX) with a Bruker XFlash detector mounted directly into the SEM.

^{27}Al magic angle spinning (MAS) nuclear magnetic resonance (NMR) experiments were carried out on an Agilent Technologies VNMRS 600 MHz spectrometer (14.1 Tesla 51 mm bore Oxford superconducting magnet) operating at a ^{27}Al Larmor frequency of 156.4 MHz, and using a 3.2 mm MAS probe head. The ^{27}Al MAS NMR spectra were recorded using a single pulse acquisition with small pulse angle ($\pi/12$), at a spinning speed of 20 kHz and with a recycle delay of 4 s. All measurements were carried out at room temperature employing $AlCl_3 \cdot 6H_2O$ as a standard reference (0 ppm). All spectra were normalized to the same area under the curves.

The acid-base characteristics of the samples were investigated on vacuum thermo-gravimetric apparatus with quartz microbalance. The concentration of acidic and basic sites was measured by the sorption of NH_3 and CO_2 in a quasi-equilibrium regime (QE-TD method of ammonia and carbon dioxide).[34] Prior to the adsorption measurements, the samples were heated under vacuum (0.133 Pa) at 773 K to reach a constant weight. The adsorption of NH_3 and CO_2 was carried out at room temperature until no uptake was observed, and the surplus was removed under vacuum. The weight was monitored during stepwise increase of temperature and vacuum treatment. The total concentration of acidic and basic sites was determined from the amount of NH_3 and CO_2 adsorbed on the sample surface at 323 K. The desorption temperature of the probe molecule was used as a criterion for the strength of acidic/basic sites [35].

The nature of acidic sites of the samples was studied by Fourier transform infrared (FT-IR) spectroscopy of adsorbed pyridine. Before adsorption/desorption experiments, the samples were pressed into thin wafers of ca. 10 mg·cm^{-2} and placed inside the FT-IR cell. The wafers were activated by calcination at 773 K for 1 h and then outgassed under vacuum at 723 K (1 Pa) for 1 h. These wafers were exposed to gaseous pyridine at 423 K. The spectra were recorded after desorption at defined temperature using Spectrum One FT-IR spectrometer (Perkin Elmer, USA) with resolution of 1 cm^{-1}, 12 scans. The reported spectra were obtained after subtraction of the background spectra recorded after calcination and prior to molecular probes adsorption.

The specific surface area of the samples was determined by a chromatographic method by thermal desorption of nitrogen on a GKh-1 instrument, with a gas mixture containing 5 vol.% of N_2 in helium.

2.3. Catalytic activity measurement

Catalytic activity tests were carried out in a fixed-bed flow quartz reactor with inner diameter of 10 mm at 523–623 K and under atmospheric pressure. Catalyst samples with grains of 1–2 mm were loaded into the reactor. Before catalytic tests, samples were treated in a gas mixture of Ar and H_2 (50:50) at 773 K for 1 h and then cooled down to the experiment temperature. Ethanol (94%, the rest – H_2O) or 1-butanol (99.8%, the rest – H_2O) feed was introduced to the hot reactor via a syringe infusion pump for evaporation. Reaction was carried out at fixed liquid hourly space velocity (LHSV). For ethanol conversion, LHSV = 0.118; 0.235; 0.47 L·L$_{cat}^{-1}$·h^{-1} (corresponding alcohol gas-hourly space velocity (GHSV) = 460; 915; 1831 h^{-1}). For 1-butanol conversion, LHSV = 0.125; 0.25; 0.5 L·L$_{cat}^{-1}$·h^{-1} (corresponding GHSV = 306; 613; 1226 h^{-1}). The mixture of Ar and H_2 with the ratio of 50:50 was used as a carrier gas with a flow of 10 mL·min^{-1}. The

reactor effluent sampling for analysis was performed only after reaching of steady state of the reaction (2 h after the beginning of catalytic experiment). The condensable liquid products were collected into an ice-water cooled receiver with a sampling interval of 1 h. The gas products after the cooled receiver were analysed with a sampling interval of 0.33 h. Catalytic indices are calculated as average values of multiple samples taken regularly during a time on stream from 2 to 4 h. The reagents and reaction products were analysed on a gas chromatograph (KristalLyuks 4000M, MetaChrome) equipped with a thermal conductivity detector and a packed column (10 % $NiSO_4$ on coal, 3 m × 3 mm) for CO and CO_2, and a flame ionization detector and a capillary column (HP-FFAP, 50 m × 0.32 mm) for organic compounds.

Catalytic activity of the catalysts was characterized by conversion (**X**), selectivity to products (**S**), yield (**Y**) and productivity (**P**):

$$X_i = \frac{n_i^0 - n_i}{n_i^0} \cdot 100\%, \quad S_j = \frac{n_j}{(n_i^0 - n_i)} \cdot 100\%,$$

$$Y_j = \frac{X_i \cdot S_j}{100\%}, \quad P_j = \frac{Y_j \cdot LHSV \cdot \rho_i \cdot k}{100\%},$$

where $\mathbf{n^0_i}$ is the initial amount of C moles of alcohol (EtOH or BuOH) in the feed; $\mathbf{n_i}$ and $\mathbf{n_j}$ are the amount of C moles of the unreacted alcohol and product **j** in the stream of the reaction products; $\boldsymbol{\rho_i}$ – liquid density of the alcohol, **k** is the maximum possible amount of the main product (**g**) that can be produced from 1 g of the alcohol.

$$S_\Sigma = \Sigma S_g, \quad Y_\Sigma = \Sigma Y_g,$$

where S_Σ, Y_Σ – sum of the selectivities and yields of resulting Guerbet alcohols **g**, namely: 1-butanol, 2-ethyl-1-butanol, 1-hexanol, 2-ethyl-1-hexanol, and 1-octanol.

3. Results and Discussion

3.1 Structural and textural characteristics

Powder X-ray patterns of as-prepared catalysts are shown in Figure 1. The patterns of synthesized precursors exhibit a series of sharp reflections for the (0 0 3), (0 0 6), (1 1 0), (1 1 3) planes and more broad peaks for the (0 0 9), (0 1 5), (0 1 8) planes, characteristic of hydrotalcite crystalline structures, which consists of layered double hydroxides with brucite-like layers.[36] After sample calcination at 873 K the patterns exhibit weak broad peaks at approximately 37°, 43°, 63°, which corresponds to diffraction of (1 1 1), (2 0 0), (2 2 0) planes and can be assigned to MgO phase (periclase) [37]. The wide peaks indicate a low crystallinity and/or small crystal sizes of the identified phases. If a separate Al-containing phase such as γ-Al_2O_3 is present, its crystallinity is too weak to be identified by XRD. It can indicate a very high dispersion of Al_2O_3 in the MgO structures with formation of Mg-Al mixed oxide periclase-like phase [38]. The formation of crystal $MgAl_2O_4$ phase is not obvious, since the main lines of spinel species can be hidden under the major MgO phase reflections if small amounts are present in the samples.

Figure 1, near here

Figure 2, near here

SEM images have been recorded to investigate the morphology of calcined samples with different Mg/Al ratios. The micrographs of the Mg-Al oxide catalysts with Mg/Al molar ratios in the range from 1 to 4 (Figure 2) show a well-developed layered structure [39,40]. One can distinguish that Al content in the samples influences the particle size and morphology. Mg-Al (4:1) sample with the highest crystallinity possesses a well-developed platelet structure typical for layered materials. It is formed by

aggregates consisting of thin plate-like crystals 150−200 nm in size. Mg-Al (3:1) and Mg-Al (2:1) samples are formed by the same aggregates. They are composed of plate-like crystals which are smaller in size (□100 nm) and significantly thinner than those in Mg-Al (4:1). Besides, the micrographs of Mg-Al (3:1) and Mg-Al (2:1) allow assuming the presence of an amorphous constituent in these samples. The images of Mg-Al (1:1) depict more amorphous aggregates; plate-like crystals are less noticeable. The uniform distribution of magnesium and aluminium on the surface of the samples with the ratio of Mg/Al = 1, 2 and 3 (EDX elemental mapping images in Figure S1, ESI) indicates the homogeneity of the prepared Mg-Al oxide system. For Mg-Al (4:1) sample, a segregation of Al to the surface can be observed.

Figure 3, near here

^{27}Al MAS NMR of the samples after treatment at 873 K has been performed in order to identify the nature of alumina species (Figure 3A). It can be noticed that two signals are observed on the spectra: one related to Al^{3+} cations tetrahedrally coordinated to oxygen (Al_{tetra}, δ = 68–83 ppm), and the other one can be assigned to Al^{3+} cations octahedrally coordinated to oxygen (Al_{octa}, δ = 11–18 ppm). The signal of Al_{octa} species consists of at least two components. Hence, the ^{27}Al MAS NMR spectra have been fitted using a Czjzek model [41] implemented in DMFit software. This model is often used [42,43] to simulate MAS experiments for quadrupolar nuclei in glassy, amorphous and disordered materials and describes the structural disorder around the probe nucleus at two or three atomic positions scale which results from a variation of the quadrupolar interaction (variation of the electronic field gradient).

Table 1, near here

The fitting results are summarized in Figure 3B and Table 1. If only three resonances are introduced in the model, the spectrum cannot be correctly fitted. Thus, fourth line located at approximately 69 ppm has been introduced. Lines located at 16–18 and 79–83 ppm may be assigned to octahedrally and tetrahedrally coordinated aluminium atoms involved in a highly dispersed Mg-containing phase (not obviously detected by XRD), and the lines at □11 and 69 ppm – to γ-alumina, as a segregated phase. It should be mentioned that only Mg-Al oxide samples with high and low amount of alumina contains such segregated γ-alumina phase.

Thus, raw synthesized precursors of Mg-Al oxide compositions constitute hydrotalcite crystalline structures, which consists of layered double hydroxides with brucite-like layers. After calcination at 873 K a very high dispersion of γ-Al_2O_3 in MgO structures with formation of Mg-Al mixed oxide periclase-like phase has been observed. The formation of $MgAl_2O_4$ is not obvious, but the presence of Mg-O-Al bonds in the samples under study is confirmed by NMR.

3.2 Acid-base properties

The acid-base characteristics (the concentration and strength of acidic and basic sites) of the Mg-Al oxide catalysts have been determined using QE-TD of ammonia and carbon dioxide. The nature of acidic sites has been studied by FT-IR spectroscopy of adsorbed pyridine.

Figure 4, near here

Figure 4 shows distribution profiles of acidic and basic sites on desorption temperature of NH_3 and CO_2, which characterizes a strength of acidic/basic sites [35]. Table 2 represents the data on acid-base capacity and surface density of the sites.

Total concentration of acidic sites in parent MgO is relatively small, and accounts for 0.15 mmol NH_3/g. The acidity spectrum of this sample includes only super weak and weak acidic sites; a limit temperature of NH_3 desorption is 473 K. Introduction of aluminium cations into MgO leads to an increase in total acidity of the Mg-Al oxide system due to the formation of a large number of medium and strong acidic sites. As a result, a limit temperature of ammonia desorption for Mg-Al oxide samples reaches 673 K. In general, when aluminium oxide is present in the system, total acidity of the samples passes through a maximum corresponding to Mg-Al (3:1) sample (C_Σ = 0.80 mmol NH_3/g). This sample is characterized by the highest concentration of strong acidic sites (0.24 mmol NH_3/g). For parent Al_2O_3, total concentration of acidic sites accounts for 0.94 mmol NH_3/g.

Table 2, near here

Since Mg-Al oxide samples have different specific surface areas, a density of acidic sites on the surfaces become an important characteristic. The obtained results (Table 2) indicate that despite an inversely proportional dependence of specific surface area on Mg/Al ratio, a change in this ratio from 4 to 1 leads to a dome-like increase in a density of acidic sites on the surface with a maximum for Mg-Al (3:1) sample. As in the case of acid capacity, a maximum acid density (6.73 μmol NH_3/m^2) corresponds to Mg-Al (3:1) sample.

Regarding basic characteristics of Mg-Al oxide system, it has been found that the introduction of aluminium cations to MgO leads to a non-monotonic dependence of total base capacity on Mg/Al ratio. The addition of a small amount of Al^{3+} (Mg-Al (4:1) sample) results in a decrease in the number of basic sites as compared with those for parent MgO. Reducing of Mg/Al ratio to 3 causes disappearance of strong basic sites, as

result, limit temperature of CO_2 desorption for Mg-Al (3:1) sample declines to 623 K. Further increase in the aluminium content contributes to disappearance of the basic sites with $T_{des.}$ = 523-623 K and formation of stronger basic sites. As a result, limit temperature of CO_2 desorption for Mg-Al (2:1) and Mg-Al (1:1) samples rises to 723 K. At the same time, medium basic sites reappear on the surface of Mg-Al (1:1) sample. For parent Al_2O_3, limit temperature of CO_2 desorption does not exceed 673 K.

Total base capacity of the samples with the ratios of Mg/Al = 1, 2 and 3 has a close order (0.21–0.3 mmol CO_2/g), but a density of surface basic sites for the various samples differs significantly. Total base density for Mg-Al oxide system varies from 2.11 to 1.34 μmol CO_2/m^2 in a non-monotonic sequence:

Mg-Al (3:1) > Mg-Al (1:1) > Mg-Al (4:1) > Mg-Al (2:1).

As mentioned in the Introduction part, for efficient Guerbet process a catalyst should have different types of sites. Table 2 shows acid/base capacity ratio (ABCR) for all investigated samples. This indicator for parent MgO has the lowest value (0.8). The addition of aluminium cations to MgO causes an increase in ABCR to 3.5. Further decrease in Mg-Al ratio leads to a decrease in acid/base capacity ratio. In general, for Mg-Al oxide compositions, when Mg/Al ratio changes from 1 to 4, a directly proportional dependence of ABCR on Mg/Al ratio is observed. For parent Al_2O_3, ABSR accounts for 3.9.

Figure 5, near here

FT-IR spectra of pyridine adsorbed on Mg-Al oxide system, MgO and Al_2O_3 are depicted in Figure 5. The bands at 1598 and 1446 cm^{-1} correspond to pyridine coordinatively bonded to weak Lewis acidic sites (LAS), as proved by their disappearance after desorption of pyridine at 473 K. In the case of magnesium oxide, the intensity of the

band at 473 K is low, which indicates a low content of LAS. The introduction of aluminium leads to an increase in the intensity of this band and, accordingly, the amount of this type of acidic sites, which confirms the previously obtained results of QE-TD. Significant changes in the transition from the sample with a lower aluminium content to the sample with its high content is not observed. The bands characteristic of pyridine adsorption on Bronsted acid sites are not detected in the spectra of all samples.

Thus, acidic and basic Lewis sites are present on the surfaces of all investigated samples; Bronsted sites are not identified. The introduction of aluminium cations into MgO leads to increase in the concentration of acidic sites, the highest content of such sites is reached for Mg-Al (3:1) sample. An increase in the concentration of basic sites is also observed in the samples with large amounts of aluminium (ratios of Mg/Al = 1, 2 and 3). The acid-base capacity ratio for Mg-Al oxide systems changes in inverse proportion to the amount of aluminium introduced into the compositions.

Summarizing the results of the acid-base characteristics studied and NMR, XRD and SEM data, the following types of acid-base Lewis pairs are assumed to be present on the surface of Mg-Al oxide systems: Mg-O-Mg (basic character) due to the presence of MgO, Al-O-Al (acidic character) due to the presence of Al_2O_3, and acid-base Lewis pairs of the Al-O-Mg type formed in the contact zone of magnesia and alumina phases during the calcination of hydrotalcites.

3.3 Catalytic properties

The main results of catalytic tests of Mg-Al oxide system (as well as parent MgO and Al_2O_3) for vapour phase condensation of EtOH to BuOH in a flow reactor at 573 K are summarized in Table 3. In the series of Mg-Al oxide catalysts (including MgO and Al_2O_3) EtOH conversion rises with an increase in the content of aluminium oxide in the samples. Addition of

aluminium oxide to magnesia lead to a slightly lower BuOH selectivity in comparison with parent MgO. However, with further increase in Al_2O_3 content the selectivity for the target product is increased passing through the maximum for Mg-Al (2:1) sample. For this catalyst 17.5 % BuOH yield is achieved (selectivity of 65.2 % at EtOH conversion of 26.9 %).

Scheme 2, near here

EtOH-to-BuOH conversion involves a complex sequence of reactions. The main steps of the Guerbet coupling are dehydrogenation of EtOH to acetaldehyde (AA), aldol self-condensation reaction to croton aldehyde (CA), hydrogenation of the condensation product to give BuOH (Scheme 1). Together with general path of the Guerbet condensation a number of side reactions also take place during the process: dehydration of EtOH to ethylene (E) and diethyl ether (DEE), disproportionation of AA to ethyl acetate (EA) by Tishchenko reaction, and others (Scheme 2).

Table 3, near here

For Mg-Al oxide catalysts under study, AA is observed in the product stream as primary product of EtOH dehydrogenation (Table 3). At the same time, aldol condensation products (i.e. CA) are generally not detected which can be attributed to the fact that this reaction occurs rapidly after initiation. DEE is the main EtOH dehydration product. Its selectivity rises with an increase in the content of aluminium oxide in the catalysts. The parent Al_2O_3 is especially selective for DEE formation (selectivity of 80.0%). Small fractions of E, acetone (Ac), EA and other side products are also identified in the product stream.

It is noteworthy that resulting BuOH reacts with itself and with initial reagent (EtOH) to form higher Guerbet alcohols. As a result, four product options exist: three

different cross-coupling products formed from the different alcohols – 2-ethyl-1-butanol (2-EB), 1-hexanol (HeOH), 1-octanol (OcOH), and a self-coupling product – 2-EH. They are detected in the reaction products with comparatively high yield. Butanal and butenes are also founded in the resulting mixture as primary products of BuOH dehydrogenation and dehydration. The composition with a ratio of Mg/Al = 4 is the most selective (24.9%) one for butenes. Therefore, Mg-Al-oxide catalysts are active not only for EtOH-to-BuOH conversion, but also for higher alcohol condensation in vapour phase.

Figure 6, near here

Overall Mg/Al ratio dependences of EtOH conversion, sum of the selectivities and yields of the main reaction products – BuOH and higher Guerbet alcohols – are summarized in Figure 6. Additionally, productivities of Mg-Al oxide system in EtOH-to-BuOH and EtOH-to-Guerbet alcohols processes are shown. According to the obtained data, selectivities and yields of BuOH and higher Guerbet alcohols have a similar trend. The best result is achieved over Mg-Al (2:1) sample providing productivity of 25 $g/(L_{cat} \cdot h)$ for BuOH and 33 $g/(L_{cat} \cdot h)$ – for total amount of Guerbet alcohols (BuOH + heavier alcohols).

A summary of catalytic properties of Mg-Al oxide system (with parent MgO and Al_2O_3 for comparison) in the process of vapour phase condensation of BuOH to 2-EH in a flow reactor at 573 K is shown in Table 4.

Table 4, near here

The dependence of catalytic properties on the ratio of Mg/Al in Mg-Al oxide composition is quite similar to the process of EtOH condensation to BuOH. With an increase in the content of aluminium oxide in the samples BuOH conversion also rises.

Selectivity of 2-EH is decreased initially with the addition of aluminium oxide as compared to parent magnesium oxide, then rises with further increase of Al_2O_3 content in the samples passing through the maximum for Mg-Al (1:1) and then again declines for parent alumina. 2-EH yield of 10.8% (selectivity of 57.3% at BuOH conversion of 18.8%) is achieved using a composition with a ratio of Mg/Al = 1 providing productivity of 19 g/(L_{cat}·h). The selectivity of BuOH dehydration products – butene and dibutyl ether (DBE) – rises with an increase in the content of Al_2O_3 in the compositions. The parent alumina is especially selective for butene and dibutyl ether formation (selectivity of 21.2 and 69.9%). Butanal is observed in the product stream as a primary product of BuOH dehydrogenation.

Figure 7, near here

Vapour phase condensation of EtOH to BuOH over the sample with the best obtained catalytic results in this process at 573 K has been also performed at different reaction temperatures (523 and 623 K). Temperature dependences of EtOH conversion, sum of the selectivities, yields and productivity to BuOH and other Guerbet alcohols for Mg-Al (2:1) composition are shown in Figure 7. EtOH conversion over the tested catalyst grows up with temperature. On the contrary, the selectivities of both BuOH and other Guerbet alcohols tend to decrease due to more active formation of side products of dehydration (E, butenes, DEE) and etherification (Ac, EA) (Table S1). The highest BuOH yield of 22.5% and productivity of 32 g/(L_{cat}·h) are observed over Mg-Al (2:1) composition at 623 K. For total amount of Guerbet alcohols these indices are 30.1% and 42 g/(L_{cat}·h).

Figure 8, near here

Figure 8 depicts temperature dependences of BuOH conversion, 2-EH selectivity, yield, and productivity of Mg-Al (1:1) and Mg-Al (2:1) compositions in vapour phase condensation of BuOH to 2-EH. BuOH conversion grows up with increasing temperature, but 2-EH selectivity is drastically decreased causing the decline of 2-EH yield. The best indices of 2-EH yield over investigated catalysts at 523 K are close: 12.7-13.2%.

In both EtOH-to-BuOH and BuOH-to-2-EH processes, the formation of dehydration (E/butenes, DEE/DBE) and dehydrogenation (AA/butanal) products is largely increased with temperature rising and vice versa (Tables S1, S2, S3).

According to thermodynamic calculations [13,44], the selectivity to BuOH (for EtOH-to-BuOH conversion) and 2-EH (for BuOH-to-2-EH one) depends on the thermodynamic features of these Guerbet condensation processes. The equilibrium yield of C-C condensation products for both processes is decreased with increasing temperature. However, for BuOH conversion such decrease is more substantial than for EtOH conversion. Therefore, BuOH-to-2-EH process is expediently carried out at lower temperature than EtOH-to-BuOH one.

Figure 9, near here

The experiments of vapour phase condensation of EtOH to BuOH and BuOH to 2-EH over the samples with the best performance have been also conducted at various LHSV at 573 K. The main catalytic indices depending on LHSV in EtOH-to-BuOH process over Mg-Al (2:1) composition are shown in Figure 9. EtOH conversion and sum of the yields of resulting Guerbet alcohols declines with rising of EtOH load, but total selectivity of Guerbet alcohols (BuOH + higher alcohols) remains at almost the same level (86.5-88.6%). Thereby, high productivity of 0.049 kg/(L_{cat}·h) for BuOH and 0.060 kg/(L_{cat}·h) for total amount of Guerbet alcohols (BuOH + heavier alcohols) is achieved at

largest (0.47 L/(L_{cat}·h)) EtOH load. It should be noted that individual BuOH selectivity is increased with the LHSV rising, conversely to selectivity of higher Guerbet alcohols, which is decreased with EtOH load (Table S4). So, at higher LHSV butanol is less involved in subsequent condensation reactions with the formation of heavier alcohols.

Figure 10, near here

The dependences of catalytic properties of Mg-Al (1:1) composition in BuOH-to-2-EH process on LHSV are depicted in Figure 10. EtOH conversion and 2-EH yield are decreased with rising of BuOH load. The selectivity of 2-EH is decreased too due to incomplete conversion of butanal and formation of side dehydration products (butenes, DBE) (Table S5). The highest productivity of Mg-Al (1:1) to 2-EH – 19 g/(L_{cat}·h) – is achieved at LHSV of 0.25 L/(L_{cat}·h).

3.4 General discussion

A number of works [17,32,33,45] are related to investigation of the mechanism of ethanol to 1-butanol conversion, however, only one theoretical paper [13] can be found about the mechanism of the 1-butanol to 2-ethyl-1-hexanol process. Let's analyse the similarities in reaction paths of these two different processes over the same series of catalysts.

Di Cosimo et al. [33] have shown that condensation of acetaldehyde is the slowest step of Guerbet reaction on mixed Mg-Al oxides. Usually the catalytic performance of Mg-Al oxide compositions in individual aldol condensation reactions is correlated with their acid-base properties, more particularly, the highest conversion is observed over compositions with the highest density of basic sites [40]. However the Guerbet reaction is a complex process with more complicated dependences. According to previous analysis of the reaction mechanism, it can be suggested that for efficient conversion of EtOH or

BuOH the catalysts should have different types of sites, meaning acidic and basic ones are equally important. The basic sites allow the Mg-Al oxide compositions to exhibit activity in key steps of the process – dehydrogenation and aldolization. Apart from that, Lewis acidic sites act like adsorption sites for intermediates. Hence, low catalytic activity of parent MgO in both EtOH-to-BuOH and BuOH-to-2-EH conversion processes (Tables 3 and 4) can be explained by the presence of predominantly isolated O^{2-} basic sites which hinder formation of the alkoxide intermediates by alcohol dissociative adsorption [32]. It is in agreement with QE-TD results (Figure 4, Table 2), where parent MgO exhibits the highest surface oxygen concentration and the highest base density. At the same time, the presence of a high density of Al^{3+}-O^{2-} pairs on a Al_2O_3 surface, in particular Lewis acidic sites, can be responsible for dehydration of ethanol to ethylene (BuOH to butenes), and the coupling with dehydration to diethyl ether (dibutyl ether) [32].

There is an interesting tendency when Mg-Al oxide samples with a high and low amount of alumina catalyse the side reactions of dehydration more effectively than the samples with middle Al content (Tables 3 and 4). Seemingly, in the catalysts with a medium amount of alumina, Al-O-Mg species (Lewis acid-base pairs) located at the surface of a brucite-like mixed oxide in an oxygen environment do not favour dehydration of EtOH to ethylene and diethyl ether. Therein, Al-O-Al species like in parent Al_2O_3 are the active sites of the dehydration [46]. This assumption is confirmed by NMR data (Figure 3, Table 1): only Mg-Al oxide samples with a high and low amount of alumina contains a segregated γ-alumina phase. Moreover, for a Mg-Al (4:1) sample, the segregation of alumina to the surface is observed by EDX mapping (Figure S1).

Figure 11, near here

Aldol self-condensation of aldehyde involves formation of carbanion species on adjacent acidic and strong basic sites, where acidic sites adsorb aldehyde molecules and basic sites abstract the proton from this aldehyde, generating a carbanion intermediate. After that, carbanion induces nucleophilic attack toward other adsorbed aldehydes, thus forming a new C–C bond and yielding an aldol product [29,33]. Such a mechanism explains the reacting of resulting butanol with itself or the initial ethanol to form 1-hexanol, 2-ethyl-1-butanol, 2-ethyl-1-hexanol, and 1-octanol.

It should be mentioned that the investigated Mg-Al oxide samples are more selective for cross-coupling (EtOH + BuOH) products – HeOH and 2-EB, than for co-condensation (BuOH + BuOH) products – 2-EH and OcOH (Table 3). It is in agreement with the classic dependence of a reaction rate on reagents concentration: since the concentration of ethanol/acetaldehyde is higher, the quantity of resulting HeOH is larger. However, a stearic or electronic effect also impacts on the relative rates of carbanion formation [17,47].

As mentioned above, the acid/base capacity ratio (ABCR) for the samples under study changes with the composition from the lowest value (0.8) for parent MgO to the highest (3.9) – for parent Al_2O_3, intermediate ABCR values correspond to Mg-Al oxide catalysts (Table 2). Therein, there are dome-like dependences of the productivity of Mg-Al oxide compositions in the EtOH → BuOH and BuOH → 2-EH processes on acid/base capacity ratio (Figure 11). An analysis of these dependencies suggests that the catalysts with a medium value of ABCR are more active and selective towards the target alcohol product (BuOH or 2-EH). The optimum acid/base capacity ratio varies from 3 to 2 with the increase in a carbon chain length of the reacting alcohol (from C_2 to C_4, i.e. from

EtOH to BuOH) during Guerbet coupling. The similar dependencies of the indices of the Guerbet process on the ratio of acidic/basic sites has been also reported for hydroxyapatites [48,49].

It is also noteworthy that the total density of acidic sites is not a critical parameter for EtOH-to-BuOH conversion. For Mg-Al (3:1) and Mg-Al (1:1) samples, total acid density values differ twice, but BuOH yields are fairly close. Hence, more important parameter is the nature of formed acid-base pairs and their availability.

For efficient realization of the BuOH-to-2-EH process, the presence of a strong basic sites is required; 2-EH selectivity is a higher for the samples with a higher content of strong basic sites (Mg-Al (1:1) and Mg-Al (2:1) samples, Table 2 and 4). However, over MgO and Mg-Al (4:1) the selectivity towards 2-EH is significantly lower than over the samples with a high aluminum content. This may be caused by a keto-enol tautomerism of the formed intermediate product or an inhibition of Meerwein−Ponndorf−Verley reduction of aldol condensation product over acid-base pairs formed by MgO. It leads to transformation of the initial alcohol into undesirable side C-C products. Over parent alumina, BuOH-to-2-EH conversion also proceeds with low selectivity. Thus, a catalyst with acidic pairs including both magnesium and aluminum cations is preferably required for BuOH-to-2-EH process.

Consequently, the acid/base capacity ratio is an important characteristic of activity and selectivity of Mg-Al oxide catalysts in the process of vapour phase condensation of ethanol to 1-butanol and 1-butanol to 2-ethyl-1-hexanol in flow. The BuOH-to-2-EH process is a quite similar to EtOH-to-BuOH conversion, but all dependences are not replicated fully. Thus, not only acid-base properties of the catalyst, but also the carbon

chain length of the reacting alcohols, an arrangement of surface active sites and other steric factors have an impact on the Guerbet condensation in vapour phase.

Conclusions

In this study the research results of the vapour phase condensation of BuOH to 2-EH over solid catalysts in a flow reactor under atmospheric pressure are presented for the first time. Conversion of EtOH and BuOH, and the selectivity towards resulting Guerbet alcohols essentially depend on the acid-base characteristics of the Mg-Al oxide system, which are determined by the Mg/Al ratio. The presence of acid-base Lewis pairs of the Al-O-Mg type, formed in the contact zone of magnesia and alumina phases during the calcination of hydrotalcites, is required for transformation of the initial alcohols into the target products (1-butanol and 2-ethyl-1-hexanol). The different optimal ratio of acidic/basic sites on the catalyst surface for conversion of EtOH to BuOH and BuOH to 2-EH may be the cause of the largest yield of BuOH (17.5% with selectivity 65.2 %) being achieved in the presence of a composition with a ratio of Mg/Al = 2, and the largest yield of 2-EH (10.8 % with selectivity 57.3 %) being obtained over a composition with the Mg/Al = 1 ratio. Additional influence on Guerbet condensation in a vapour phase has the carbon chain length of the reacting alcohols and an arrangement of active sites on the surface. The potential opportunity of the 2-ethyl-1-hexanol production from ethanol using the successive Guerbet condensation EtOH → BuOH and BuOH → 2-EH in a flow reactor under atmospheric pressure over Mg-Al oxide catalytic systems has been shown.

Acknowledgements

This work was financially supported by programs of National Academy of Sciences of Ukraine KPKVK 6541230 “Support for the development of priority areas of scientific research”. The authors, in particular O.V. Larina, K.V. Valihura, D.Yu. Balakin, I. Khalakhan and T. Čendak acknowledge CERIC-ERIC Consortium for access to experimental facilities at Nuclear Magnetic Resonance Spectrometer “Magic” at Slovenian NMR Centre (Proposal number: 20182046) and Field Emission Scanning Electron Microscope at Charles University in Prague (Proposal number: 20182124), and financial support.

References

[1] J.M.R. Gallo, J.M.C. Bueno, U. Schuchardt, J. Braz. Chem. Soc. 25 (2014) 2229–2243.

[2] J. Sun, Y. Wang, ACS Catal. 4 (2014) 1078–1090.

[3] J.A. Posada, A.D. Patel, A. Roes, K. Blok, A.P.C. Faaij, M.K. Patel, Bioresour. Technol. 135 (2013) 490–499.

[4] W. Michaels, H. Zhang, W.L. Luyben, J. Baltrusaitis, Biomass and Bioenergy 109 (2018) 231–238.

[5] G. Knothe, Lipid Technol. (2002) 101–104.

[6] M. Guerbet, Comptes Rendus l'Académie Des Sci. 128 (1899) 511.

[7] A.J. O'Lenick Jr., J. Surfactants Deterg. 4 (2001) 311–315.

[8] C. Angelici, B.M. Weckhuysen, P.C.A. Bruijnincx, ChemSusChem 6 (2013) 1595–1614.

[9] L. Wu, T. Moteki, A.A. Gokhale, D.W. Flaherty, F.D. Toste, Chem 1 (2016) 32–58.

[10] A. Wick, E.U. Mahnke, Method for Producing Guerbet Alcohols, US 8779216 B2, 2014.

[11] S. Thach, R. Shong, V. Dwarakanath, G. Winslow, Method of Manufacture of Guerbet Alcohols For Making Surfactants Used In Petroleum Industry Operations, US 20130068457 A1, 2013.

[12] S. Thach, R. Shong, V. Dwarakanath, G. Winslow, Alcools de Guerbet En Tant Que Substituts de La Vaseline, WO 2013120757 AI, 2013.

[13] D. Gabriëls, W.Y. Hernández, B. Sels, P. Van Der Voort, A. Verberckmoes, Catal. Sci. Technol. 5 (2015) 3876–3902.

[14] W.R. da S. Trindade, R.G. dos Santos, Renew. Sustain. Energy Rev. 69 (2017) 642–651.

[15] Q. Zhang, J. Dong, Y. Liu, Y. Wang, Y. Cao, J. Energy Chem. 25 (2016) 907–910.

[16] M.O.S. Dias, L.G. Pereira, T.L. Junqueira, L.G. Pavanello, M.F. Chagas, O. Cavalett, R. Maciel Filho, A. Bonomi, Chem. Eng. Res. Des. 92 (2014) 1441–1451.

[17] J.T. Kozlowski, R.J. Davis, ACS Catal. 3 (2013) 1588–1600.

[18] A.D. Patel, S. Telalović, J.H. Bitter, E. Worrell, M.K. Patel, Catal. Today 239 (2015) 56–79.

[19] C.A. Hamilton, S.D. Jackson, G.J. Kelly, Appl. Catal. A Gen. 263 (2004) 63–70.

[20] Y. Li, X. Liu, H. An, X. Zhao, Y. Wang, Ind. Eng. Chem. Res. 55 (2016) 6293–6299.

[21] N. Liang, X. Zhang, H. An, X. Zhao, Y. Wang, Green Chem. 17 (2015) 2959–2972.

[22] S.C. Patankar, G.D. Yadav, Catal. Today 291 (2017) 223–233.

[23] C. Carlini, A. Macinai, A.M. Raspolli Galletti, G. Sbrana, J. Mol. Catal. A Chem. 212 (2004) 65–70.

[24] R. Miller, G. Bennett, Ind. Eng. Chem. 53 (1961) 33–36.

[25] C. Carlini, M. Marchionna, M. Noviello, A.M. Raspolli Galletti, G. Sbrana, F. Basile, A. Vaccari, J. Mol. Catal. A Chem. 232 (2005) 13–20.

[26] T. Matsu-ura, S. Sakaguchi, Y. Obora, Y. Ishii, J. Org. Chem. 71 (2006) 8306–8308.

[27] K.K. Ramasamy, M. Gray, H. Job, D. Santosa, X.S. Li, A. Devaraj, A. Karkamkar, Y. Wang, Top. Catal. 59 (2016) 46–54.

[28] K.K. Ramasamy, M. Gray, H. Job, C. Smith, Y. Wang, Catal. Today 269 (2016) 82–87.

[29] D.L. Carvalho, R.R. de Avillez, M.T. Rodrigues, L.E.P. Borges, L.G. Appel, Appl. Catal. A Gen. 415–416 (2012) 96–100.

[30] M. León, E. Díaz, S. Ordóñez, Catal. Today 164 (2011) 436–442.

[31] S. Ordóñez, E. Díaz, M. León, L. Faba, Catal. Today 167 (2011) 71–76.

[32] J.I. Di Cosimo, V.K. Diez, M. Xu, E. Iglesia, C.R. Apesteguıa, J. Catal. 178 (1998) 499–510.

[33] J.I. Di Cosimo, C.R. Apesteguıa, M.J.L. Ginés, E. Iglesia, J. Catal. 190 (2000) 261–275.

[34] N. V. Vlasenko, Y.N. Kochkin, A.M. Puziy, J. Mol. Catal. A Chem. 253 (2006) 192–197.

[35] G.I. Kapustin, T.R. Brueva, Thermochim. Acta 379 (2001) 71–75.

[36] D.G. Cantrell, L.J. Gillie, A.F. Lee, K. Wilson, Appl. Catal. A Gen. 287 (2005) 183–190.

[37] K.J.D. MacKenzie, R.H. Meinhold, B.L. Sherriff, Z. Xu, J. Mater. Chem. 3 (1993) 1263–1269.

[38] R.J. Chimentão, S. Abelló, F. Medina, J. Llorca, J.E. Sueiras, Y. Cesteros, P. Salagre, J. Catal. 252 (2007) 249–257.

[39] Z. Xu, G. Lu, Chem. Mater. (2005) 1055–1062.

[40] O. Kikhtyanin, L. Čapek, L. Smoláková, Z. Tišler, D. Kadlec, M. Lhotka, P. Diblíková, D. Kubička, Ind. Eng. Chem. Res. 56 (2017) 13411–13422.

[41] J.B. d'Espinose de Lacaillerie, C. Fretigny, D. Massiot, J. Magn. Reson. 192 (2008) 244–251.

[42] F. Hosoglu, J. Faye, K. Mareseanu, G. Tesquet, P. Miquel, M. Capron, O. Gardoll, J.F. Lamonier, C. Lamonier, F. Dumeignil, Appl. Catal. A Gen. 504 (2015) 533–541.

[43] S. Barama, C. Dupeyrat-Batiot, M. Capron, E. Bordes-Richard, O. Bakhti-Mohammedi, Catal. Today 141 (2009) 385–392.

[44] J. Scalbert, F. Thibault-Starzyk, R. Jacquot, D. Morvanb, F. Meuniera, J. Catal. 311 (2014) 28–32.

[45] C.R. Ho, S. Shylesh, A.T. Bell, ACS Catal. 6 (2016) 939–948.

[46] C.T. Fishel, R.J. Davis, Langmuir 10 (1994) 159–165.

[47] H. Tsuji, F. Yagi, H. Hattori, H. Kita, J. Catal. 148 (1994) 759–770.

[48] L. Silvester, J.F. Lamonier, J. Faye, M. Capron, R.N. Vannier, C. Lamonier, J.L. Dubois, J.L. Couturier, C. Calais, F. Dumeignil, Catal. Sci. Technol. 5 (2015) 2994–3006.

[49] L. Silvester, J.F. Lamonier, C. Lamonier, M. Capron, R.N. Vannier, A.S. Mamede, F. Dumeignil, ChemCatChem 9 (2017) 2250–2261.

Captions for Figures and Scheme

Figure 1: XRD of the prepared samples before (a) and after treatment at 873 K (b): 1 – MgO, 2 – Mg-Al (4:1), 3 – Mg-Al (3:1), 4 – Mg-Al (2:1), 5 – Mg-Al (1:1); 6 – Al_2O_3.

Figure 2: SEM images of the samples after a treatment at 873 K: A – Mg-Al (4:1), B – Mg-Al (3:1), C – Mg-Al (2:1), D – Mg-Al (1:1).

Figure 3: ^{27}Al MAS NMR spectra of the samples after a treatment at 873 K (A) and the corresponding fit calculating using DMFit software (B): 1 – Mg-Al (4:1), 2 – Mg-Al (3:1), 3 – Mg-Al (2:1), 4 – Mg-Al (1:1).

Figure 4: Differential QE-TD-curves of ammonia (A) and carbon dioxide (B) for the samples: 1 – MgO, 2 – Mg-Al (4:1), 3 – Mg-Al (3:1), 4 – Mg-Al (2:1), 5 – Mg-Al (1:1), 6 – Al_2O_3.

Figure 5: FTIR spectra of adsorbed pyridine over the samples after desorption at 423 K (dash lines) and 473 K (solid lines): 1 – MgO, 2 – Mg-Al (4:1), 3 – Mg-Al (3:1), 4 – Mg-Al (2:1), 5 – Mg-Al (1:1); 6 – Al_2O_3.

Figure 6: Mg/Al ratio dependences of EtOH conversion, sum of the selectivities and yields of resulting Guerbet alcohols, and productivity of Mg-Al oxide compositions in EtOH-to-BuOH and EtOH-to-Guerbet alcohols processes (T = 573 K, LHSV = 0.235 $L/(L_{cat} \cdot h)$).

Figure 7: Temperature dependences of EtOH conversion, sum of the selectivities and yields of resulting Guerbet alcohols, and productivity of Mg-Al (2:1) composition in EtOH-to-BuOH and EtOH-to-Guerbet alcohols processes (LHSV = 0.235 $L/(L_{cat} \cdot h)$).

Figure 8: Temperature dependences of BuOH conversion, 2-EH selectivity and yield, and productivity of Mg-Al (1:1) (A) and Mg-Al (2:1) (B) compositions in BuOH-to-2-EH process (LHSV = 0.250 L/(L_{cat}·h)).

Figure 9: LHSV dependences of EtOH conversion, sum of the selectivities and yields of resulting Guerbet alcohols, and productivity of Mg-Al (2:1) composition in EtOH-to-BuOH and EtOH-to-Guerbet alcohols processes (T = 573 K).

Figure 10: LHSV dependences of BuOH conversion, 2-EH selectivity and yield, and productivity of Mg-Al (1:1) composition in BuOH-to-2-EH process (T = 573 K).

Figure 11: Dependence of the productivity of Mg-Al oxide composition in EtOH → BuOH and BuOH → 2-EH processes on acid/base capacity ratio.

Scheme 1: Guerbet reaction mechanism: 1 - dehydrogenation of initial alcohol to aldehyde, 2 - aldol self-condensation reaction of aldehyde, 3 -dehydration of the aldol product to unsaturated aldehyde, 4 - hydrogenation (and/or Meerwein−Ponndorf−Verley reduction) of the unsaturated aldehyde to give resulting alcohol.

Scheme 2. Side reactions during Guerbet process of EtOH condensation.

Table 1. ^{27}Al NMR analysis of Mg-Al oxide compositions.

Samples	Area, %			
	$Al_{octa\ 1}$, δ = 11 ppm	$Al_{octa\ 2}$, δ = 16–18 ppm	$Al_{tetra\ 1}$, δ = 69 ppm	$Al_{tetra\ 2}$, δ = 79–83 ppm
Mg-Al (4:1)	6.8	49	12	32
Mg-Al (3:1)	1.2	58	-	40
Mg-Al (2:1)	-	51	-	49
Mg-Al (1:1)	12	59	8.3	20

Table 2. Acid-base characteristics of the Mg-Al oxide catalysts.

Characteristics	Sites[1]	Catalyst samples					
		MgO [71 m^2/g]	Mg-Al (4:1) [88 m^2/g]	Mg-Al (3:1) [119 m^2/g]	Mg-Al (2:1) [157 m^2/g]	Mg-Al (1:1) [165 m^2/g]	Al_2O_3 [199 m^2/g]
Acid capacity, mmol NH_3/g	sw	0.06	0.17	0.24	0.16	0.05	0.32
	w	0.09	0.16	0.32	0.25	0.28	0.39
	m	-			0.06	0.12	
	s	-	0.13	0.24	0.14	0.13	0.23
	Total	0.15	0.46	0.80	0.61	0.58	0.94
Acid density, µmol NH_3/m^2	sw	0.85	1.93	2.02	1.02	0.30	1.61
	w	1.27	1.82	2.69	1.59	1.70	1.96
	m	-			0.38	0.73	
	s	-	1.48	2.02	0.89	0.79	1.16
	Total	2.12	5.23	6.73	3.88	3.52	4.72
Base capacity, mmol CO_2/g	sw	0.01	0.02	0.09	0.03	0.02	0.07
	w_1	0.04	0.03	0.07	0.08	0.15	0.10
	w_2				0.05		
	m	0.08	0.05	0.09	-	0.07	0.04
	s	0.05	0.03	-	0.05	0.06	0.03
	Total	0.18	0.13	0.25	0.21	0.30	0.24
Base density, µmol CO_2/m^2	sw	0.14	0.23	0.76	0.19	0.12	0.35
	w_1	0.56	0.34	0.59	0.51	0.91	0.50
	w_2				0.32		
	m	1.13	0.57	0.76	-	0.42	0.20
	s	0.70	0.34	-	0.32	0.36	0.15
	Total	2.53	1.48	2.11	1.34	1.81	1.21
Acid-base capacity ratio		0.8	3.5	3.2	2.9	1.9	3.9

[1] Abbreviations: "sw" – super weak sites, "w" – weak sites, "m" – medium sites, "s" – strong sites.

Table 3. Indices of EtOH-to-BuOH conversion over the Mg-Al oxide catalysts.[a]

Catalyst	Conversion, %	Selectivity, %[b]															BuOH Yield, %	Carbon balance, %
		BuOH	2-EB	HeOH	OcOH	2-EH	E	Butenes	DEE	C_{2-4}	AA	Ac	EA	Butanal	CA	C_{5+}		
MgO	6.7	38.4	1.0	1.9	1.1	0.6	<0.5	<0.5	<0.5	12.7	6.5	1.1	<0.5	4.0	<0.5	31.2	2.6	85
Mg-Al (4:1)	8.9	37.6	<0.5	1.2	<0.5	0.7	<0.5	24.9	4.0	4.3	7.0	2.6	3.4	2.8	<0.5	9.6	3.3	91
Mg-Al (3:1)	22.8	64.1	3.8	8.7	1.7	2.5	<0.5	1.4	0.6	2.0	3.9	<0.5	1.7	0.7	<0.5	8.1	14.6	94
Mg-Al (2:1)	26.9	65.2	4.9	11.4	2.1	2.9	<0.5	<0.5	0.6	<0.5	2.9	<0.5	2.2	<0.5	<0.5	6.5	17.5	95
Mg-Al (1:1)	28.6	51.0	2.7	6.6	0.6	1.9	1.2	5.1	10.8	1.9	7.1	1.5	2.2	2.0	<0.5	5.1	14.6	92
Al_2O_3	41.5	6.7	<0.5	<0.5	<0.5	<0.5	2.5	2.2	80.0	5.1	1.8	<0.5	<0.5	<0.5	<0.5	<0.5	2.8	85

[a] T = 573 K, LHSV = 0.235 $L \cdot L_{cat}^{-1} \cdot h^{-1}$.

[b] The selectivities reported in the table are normalized.

Table 4. Indices of BuOH-to-2-EH conversion over the Mg-Al oxide catalysts. [a]

Catalyst	Conversion, %	Selectivity, %[b]					2-EH Yield, %	P, g/(L_{cat} · h)	Carbon balance, %
		2-EH	Butenes	Butanal	DBE	Others			
MgO	13.0	27.9	<0.5	18.0	1.1	52.5	3.6	6	85
Mg-Al (4:1)	10.5	10.0	3.5	19.4	7.1	60.0	1.0	2	88
Mg-Al (3:1)	13.6	47.7	0.7	19.7	6.9	25.0	6.5	11	90
Mg-Al (2:1)	17.3	56.7	0.9	14.2	12.3	15.9	9.8	17	88
Mg-Al (1:1)	18.8	57.3	1.0	13.1	12.0	16.6	10.8	19	93
Al_2O_3	44.2	1.2	21.1	2.9	69.9	4.9	0.5	1	85

[a] T = 573 K, LHSV = 0.250 $L \cdot L_{cat}^{-1} \cdot h^{-1}$.

[b] The selectivities reported in the table are normalized.

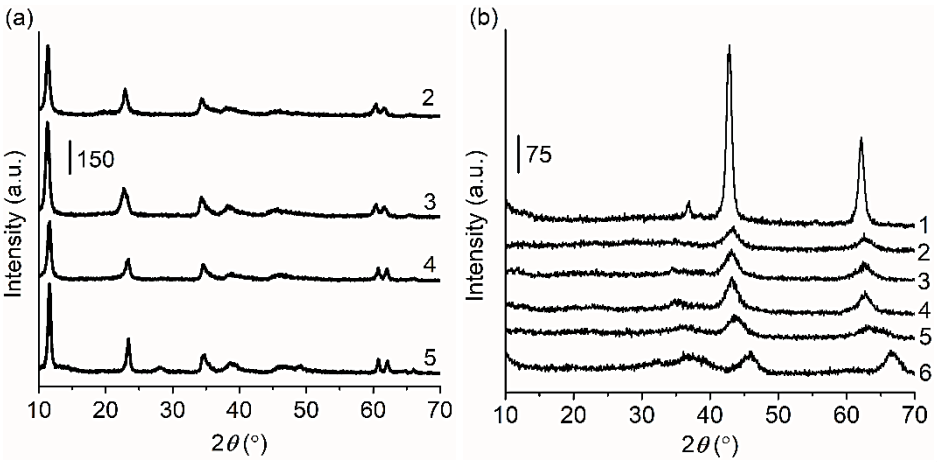

Figure 1

(A)

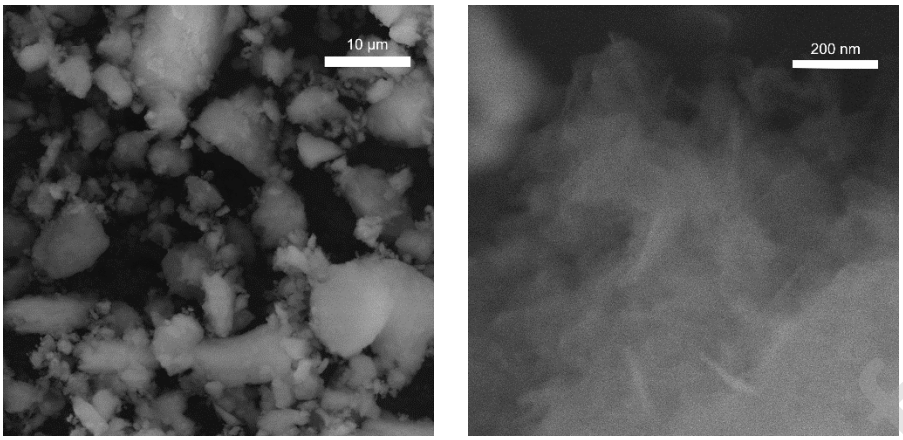

(B)

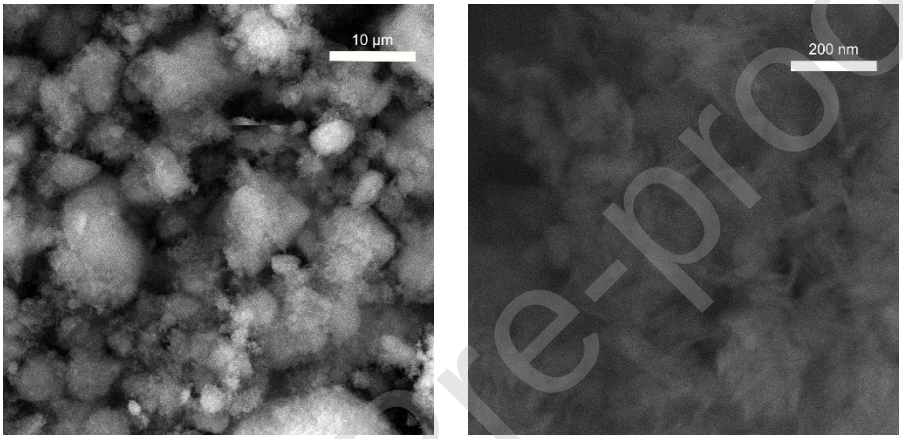

(C)

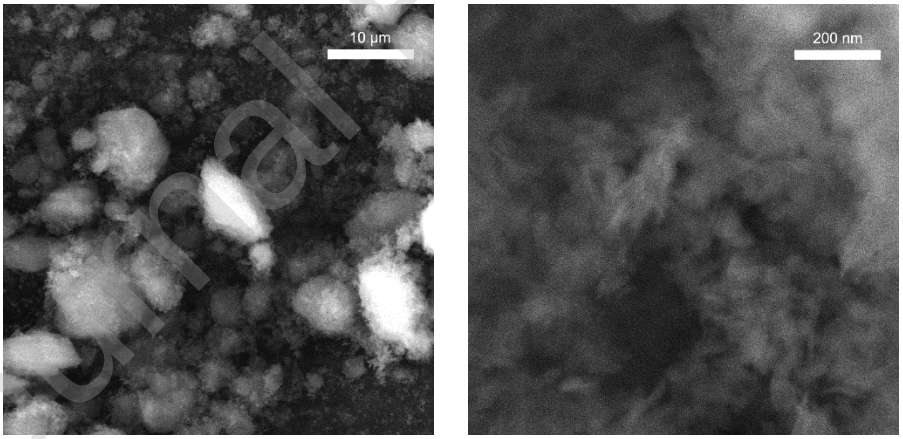

(D)

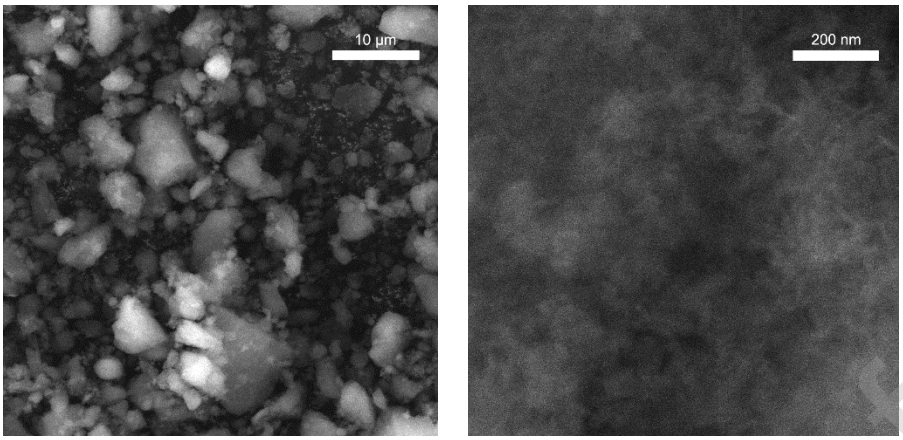

Figure 2

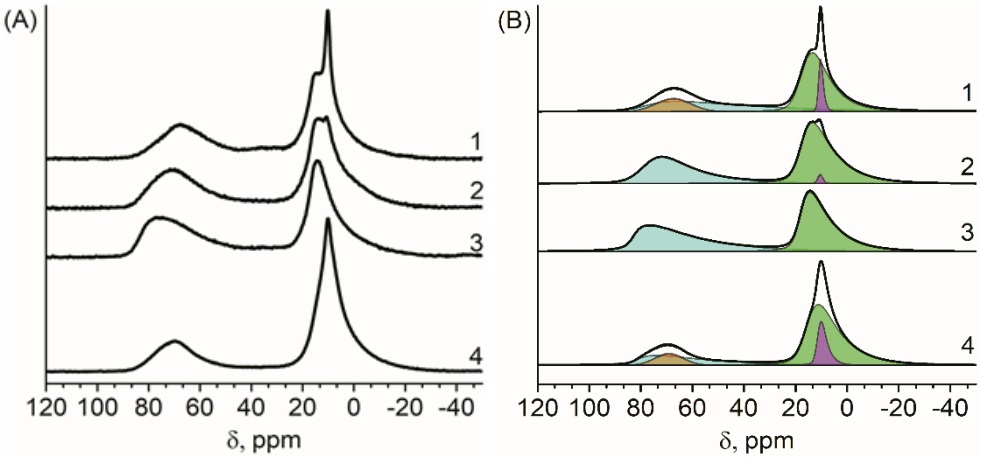

Figure 3

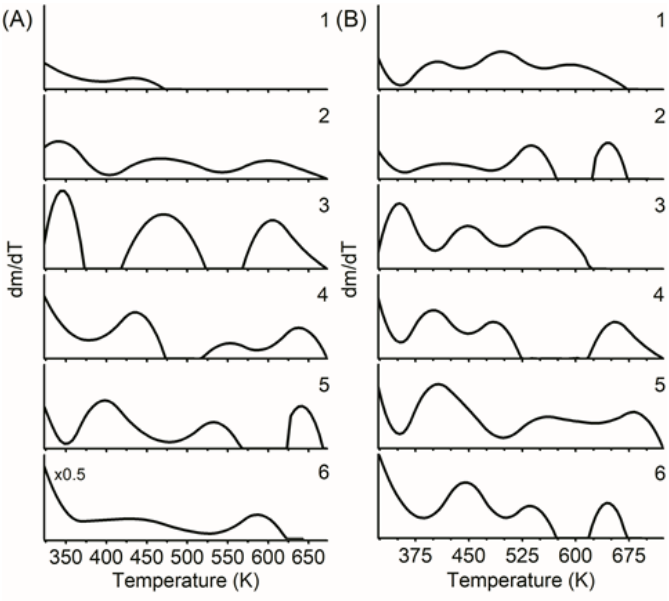

Figure 4

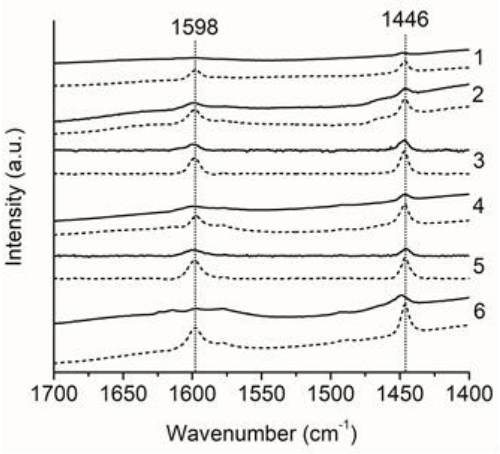

Figure 5

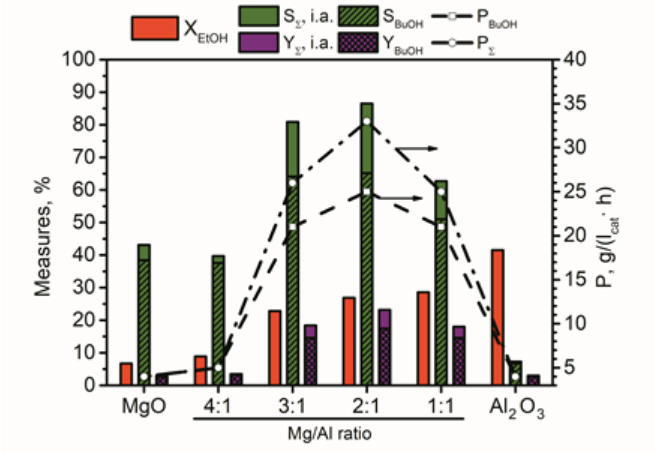

Figure 6

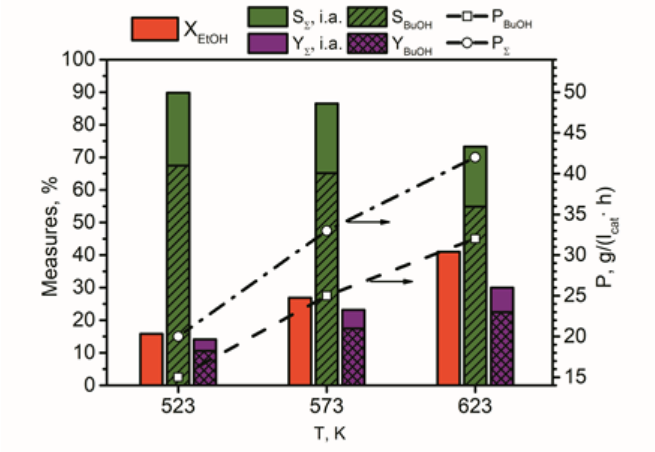

Figure 7

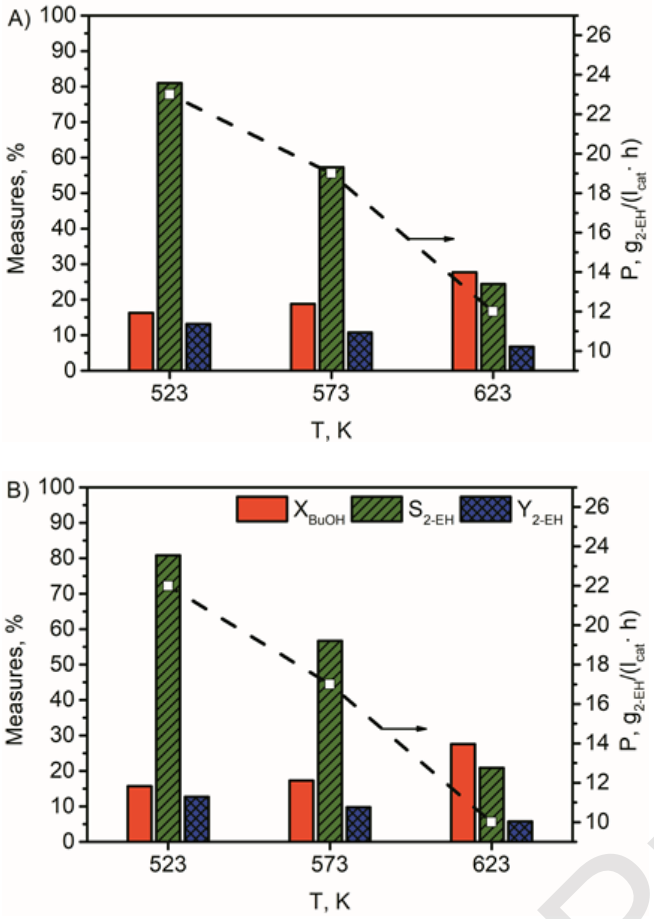

Figure 8

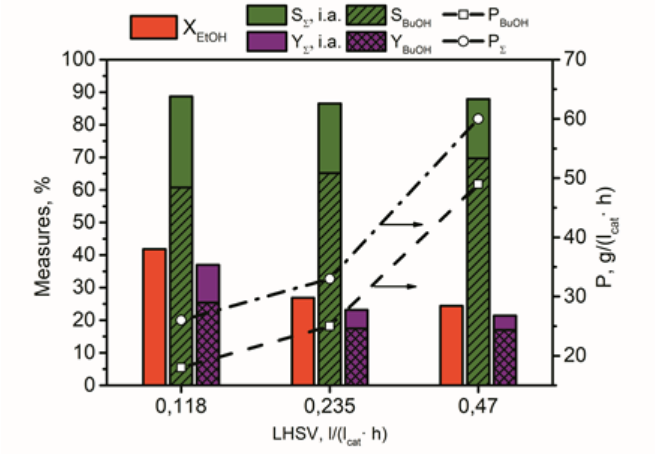

Figure 9

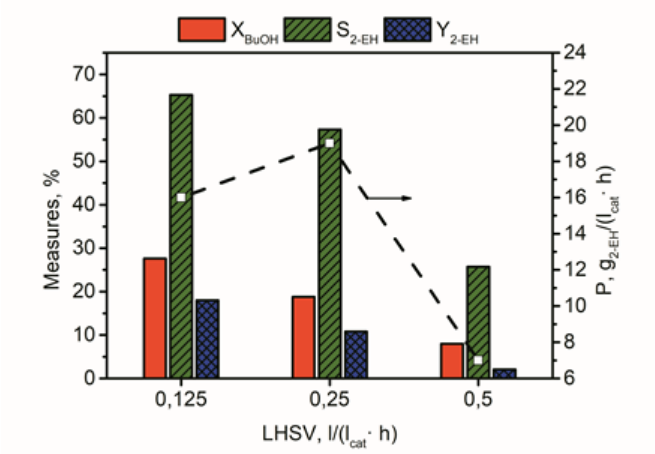

Figure 10

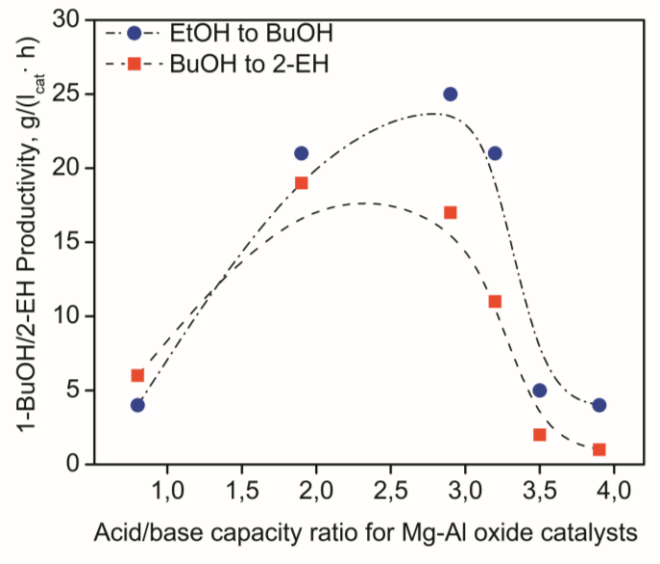

Figure 11

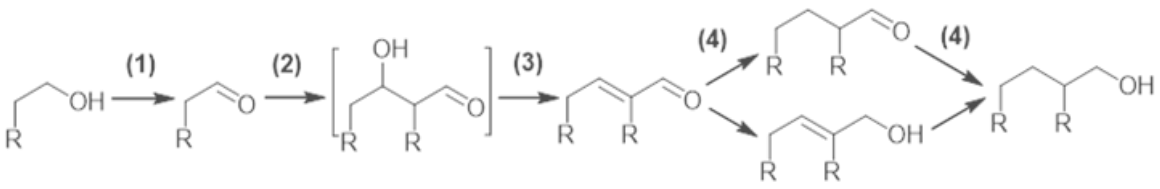

Scheme 1

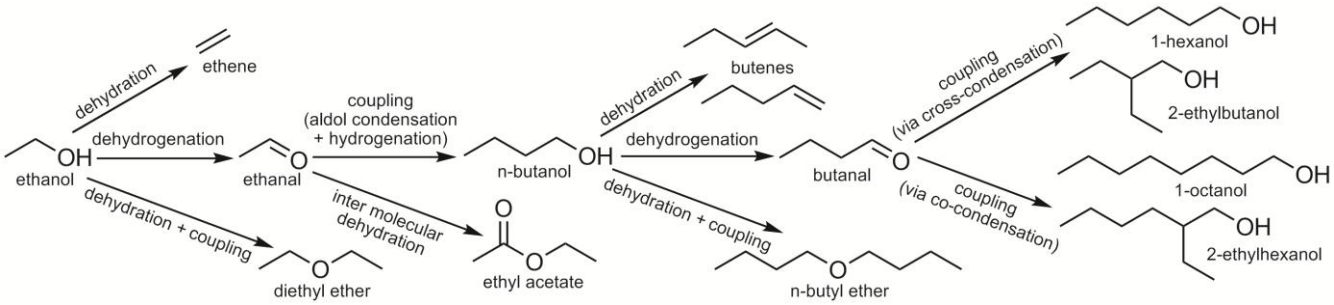

Scheme 2